Wave correlation approaches to analyse vectorial velocity fields: application to a honeycomb core sandwich panel

Q. Leclère [1], **F. Marchetti** [2], **N. B. Roozen** [3], **K. Ege** [1], **M. Kersemans** [4]
[1] Univ. Lyon, INSA Lyon, LVA,
F-69621, Villeurbanne, France

[2] Matelys - Research Lab,
F-69120 Vaulx-en-Velin, France

[3] KU Leuven, Department of Physics and Astronomy, Soft Matter and Biophysics, Laboratory of Acoustics, Celestijnenlaan 200D, 3001 Leuven, Belgium.

[4] Ghent Univ, Mechanics of Materials and Structures,
Technologiepark 46, B-9052 Zwijnaarde, Belgium

Abstract
Last decades wave correlation methods have been developed for the analysis of structural vibrations. The high spatial resolution that can be obtained nowadays by scanning laser vibrometry offers very dense measurement grids allowing the characterization of vibrating structures over a very wide frequency range. The principle of wave correlation approaches is to calculate the correlation between the vibration field measured at a given frequency and a vibrational field computed by means of an analytical model. The study reported in the present work concerns the application of wave correlation techniques to vectorial velocity fields (i.e. the 3D velocity vector measured on a 2D grid). The measurement of the tangential components of the velocity of the structure gives access to waves associated to in-plane motion, involving membrane and shearing deformation. A specific processing is required to correctly interpret such data, in order to properly separate the different wave types and to extract their specific dispersion laws.

1 Wave correlation

The idea of wave correlation approaches is to compare a measured field $f(x,\omega)$ captured at a given set of observation points x depending on the frequency ω to an analytic representation of the field provided by a wave solution of the medium $g(x,\xi)$. A general expression of the correlation reads

$$\gamma^2(\omega,\xi) = \frac{|\langle f(x,\omega), g(x,\xi)\rangle|^2}{\|f(x,\omega)\|^2\|g(x,\xi)\|^2}, \tag{1}$$

where $\langle,\rangle$ represents the scalar product and where ξ stands for the set of parameters describing the wave. At a given frequency ω, the correlation is calculated for a wide range of potential wave parameter sets ξ, significant maxima implying an actual contribution of the corresponding wave. Note that Eq. 1 is used for numerous applications in vibration and acoustics testing, one may cite the Modal Assurance Criterion where wave solutions are calculated modes, or acoustic beamforming where acoustic waves on the microphone array are parameterized typically by a direction of arrival.

When dealing with a scalar (mono-component) vibration field measured on a surface (typically the normal velocity measured on a plane structure), the waveform can be either 'plane' [1] (which is usually valid at some distance from the source) or 'cylindrical' [2] (which is a better approximation of the vibrational field close to a point source). In the specific case where the waves are plane, the scalar product is equivalent to

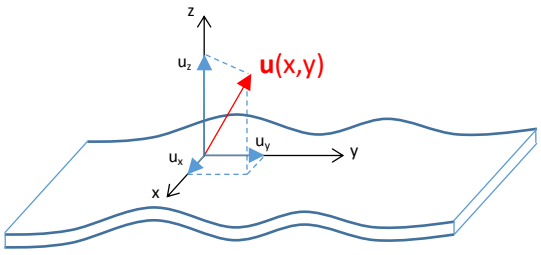

Figure 1: Scheme of the vectorial velocity field and associated coordinate system.

a 2D Fourier Transform, wavenumbers k_x and k_y being the wave parameters. If the measurement grid is rectangular and regular, the 2D DFT is given by

$$U(k_x, k_y) = \sum_{x,y} u(x,y) e^{-jk_x x} e^{-jk_y y}. \tag{2}$$

When the velocity of the structure is measured not only in the normal direction as a scalar quantity but also in the two in-plane directions as a vectorial quantity (see Fig. 1), the scalar product of the correlation formula has to include all three directions. The considered plane wave types may thus mix the displacements along the three directions. For instance, the flexural wave induces an in-plane displacement related to the rotation of the cross section. In-plane waves are characterized by a vibration either along or perpendicular to the propagation direction (compression/longitudinal and transverse waves, respectively). The compression wave also generates an out of plane displacement by Poisson's effect. These three wave types may be written as follows

$$\mathbf{F} = \left\{ \begin{array}{c} -\alpha i k_x \\ -\alpha i k_y \\ 1 \end{array} \right\} e^{ik_x x} e^{ik_y y}\ ,\ \mathbf{L} = \left\{ \begin{array}{c} \cos(\theta) \\ \sin(\theta) \\ -\alpha \nu i k \end{array} \right\} e^{ik_x x} e^{ik_y y}\ ,\ \mathbf{T} = \left\{ \begin{array}{c} -\sin(\theta) \\ \cos(\theta) \\ 0 \end{array} \right\} e^{ik_x x} e^{ik_y y}, \tag{3}$$

where $k = \sqrt{k_x^2 + k_y^2}$, $\cos(\theta) = k_x/k$, $\sin(\theta) = k_y/k$. α is a coupling coefficient, standing for the half-thickness of the plate, at least for a low-frequency and homogeneous modelling (thin plate, no shearing). At mid or high frequencies, and for multi-layer plates, a tuning of this coefficient may be necessary.

Denoting the Fourier coefficients of the 3 components of the vibration field $\mathbf{u}$ by U_x, U_y, and $U_z(k_x, k_y)$, one can write, at a given frequency ω and for each wavenumber plane coordinate (k_x, k_y) [1]

$$\begin{array}{rll} \gamma_F^2 & \propto |\langle \mathbf{u}, \mathbf{F} \rangle|^2 = & |U_z + \alpha i k_x U_x + \alpha i k_y U_y|^2 \\ \gamma_L^2 & \propto |\langle \mathbf{u}, \mathbf{L} \rangle|^2 = & |\cos(\theta) U_x + \sin(\theta) U_y + i\alpha\nu k U_z|^2 \\ \gamma_T^2 & \propto |\langle \mathbf{u}, \mathbf{T} \rangle|^2 = & |-\sin(\theta) U_x + \cos(\theta) U_y|^2 \end{array} \tag{4}$$

It is worth noting that, because of in-plane and transverse coupling ($\alpha > 0$), the flexural and longitudinal propagation modes are not orthogonal. The coherence between these two modes can be calculated as:

$$\gamma_{LF}^2 = \frac{|\langle \mathbf{L}, \mathbf{F} \rangle|^2}{\|\mathbf{L}\|^2 \|\mathbf{F}\|^2} = \frac{(1-\nu)^2 \alpha^2 k^2}{(\alpha^2 k^2 + 1)(\alpha^2 k^2 \nu^2 + 1)}, \tag{5}$$

[1] Note that the inner product involves the complex conjugate operation on the second input function.

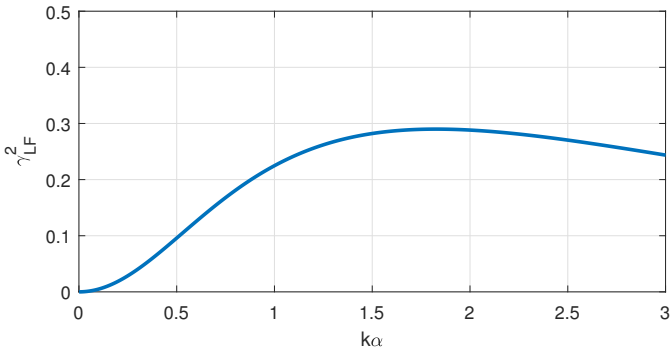

Figure 2: Correlation between flexural and longitudinal waves caused by in-plane and out of plane motion coupling effects.

The flexural and transversal components, and the transversal and longitudinal components are orthogonal to each other, resulting in coherences that remain null: $\gamma^2_{TF} = \gamma^2_{TL} = 0$.
The coherence γ^2_{LF} is drawn in Fig. 2 for $k\alpha < 3$ and $\nu = 0.3$. It can be seen that the correlation coefficient between the two waves can reach values up to 0.25 to 0.3 for $k\alpha > 1$. However, ambiguities that could result from this correlation is expected to be cleared up by the fact that their wavenumber signatures are expected to be significantly different in most cases.

2 Application to a honeycomb core composite panel

2.1 Experimental setup

The studied sample is a rectangular ($52 \times 73cm^2$) composite panel made of two aluminium plates (thickness 0.6mm) encapsulating a nomex honeycomb core (thickness 9mm). A piezoelectric actuator is glued around the center of the sample. The sample is supported by means of elastic ropes that are connected to a frame, thus approximating free-free boundary conditions. The vectorial velocity field is measured using a 3D laser vibrometer, scanning a regular and rectangular grid of 187×270 points (spatial resolution of 2mm).

2.2 Wavenumber content of measured fields

The wavenumber spectra of velocity fields at 49kHz, a frequency close to the upper bound of the studied frequency range, are shown in Fig. 3. Wavenumber circles corresponding to different propagation modes clearly appear, with different magnitudes in the three directions. Circles at the low wavenumbers, that correspond to compression and transverse in-plane propagation modes, are logically more energetic on the k-maps of in-plane motion, but also appear on both the U_x and U_y directions. The high wavenumber circle, more energetic on the out-of-plane vibration, correspond logically to the flexural waves. However, it is also quite strongly contributing to in-plane motion, because of the coupling coefficient α discussed in the previous section.

To contruct the wavenumber distribution as a function of the frequency, an average power for a wavenumber k at each frequency is obtained by interpolating and averaging the maps on a circle of radius k. The results for U_x, U_y, and U_z are shown in Fig. 4. The three circles visible in Fig. 3 correspond to three different ridges that clearly appear in the $k - f$ maps, following the dispersion laws of the different propagation modes. The two ridges in the low wavenumber domain for which the wavenumber is proportional to frequency correspond to longitudinal and transverse in-plane motions, mainly visible in the x and y directions. The ridges at higher wavenumbers for which the wavenumber is not proportional to frequency correspond to the flexural waves, mainly contributing to z motion but also noticeable in the x and y motions over the whole frequency range. Note that this particular ridge correspond to an elliptic profile in the wavenumber plane

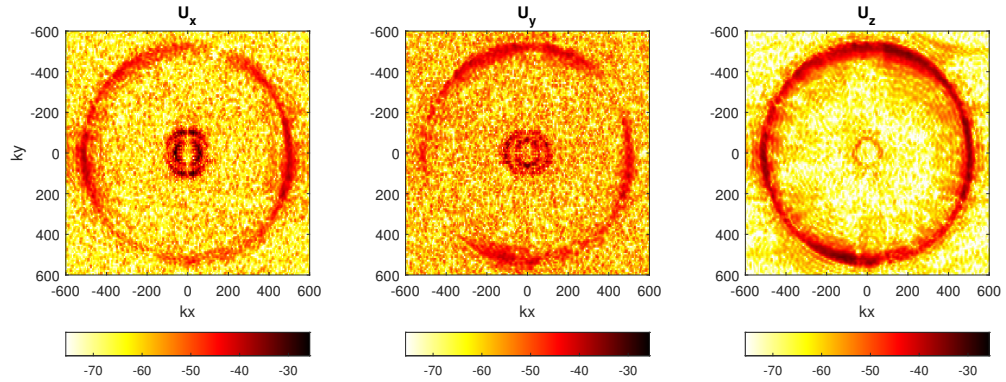

Figure 3: Wavenumber representation of U_x, U_y and U_z at 49kHz.

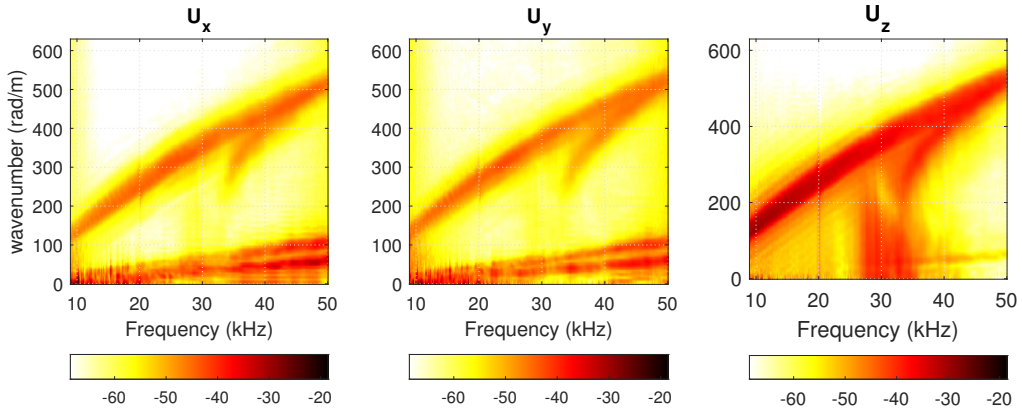

Figure 4: Frequency-Wavenumber map of U_x, U_y and U_z.

(Fig. 3), due to an orthotropicity of the core material, which explains a widening of the ridge in Fig. 4. Moreover, something emerges on the z direction at lower wavenumbers around and above 30kHz, where a fourth ridge seems to appear and to join the flexural ridge when increasing the frequency. This ridge may be related to an antisymmetric flexural behavior of the skins, as it will be discussed in section 2.4.

2.3 Correlation indicator for Longitudinal, Transversal and Flexural waves

The wave correlation for the three wave propagation types, calculated by means of Eq. 4, are drawn in Fig. 5 for a frequency of 49kHz. Note that the α coefficient being not known a priori for such structures, its value is initially set to 0. Its estimation from measurements is discussed in section 2.5.

A first observation is that the two circles at low wavenumbers, corresponding to in-plane longitudinal and transverse modes, are very well separated : the first circle with the lowest wavenumber appears only on the longitudinal coherence, while the second one with a slightly higher wavenumber appears only on the transverse coherence map. A second observation concerns the contribution of the flexural waves to the longitudinal and transverse coherences. The flexural wave circle, that was similarly contributing to U_x and U_y in Fig. 3, is now much more energetic on the longitudinal coherence than on the transverse one (of about 10 to 20dB). This is logical, because the in-plane motion caused by the rotation of the cross section is generated along the propagation direction of the flexural wave. Theoretically, the flexural wave should not

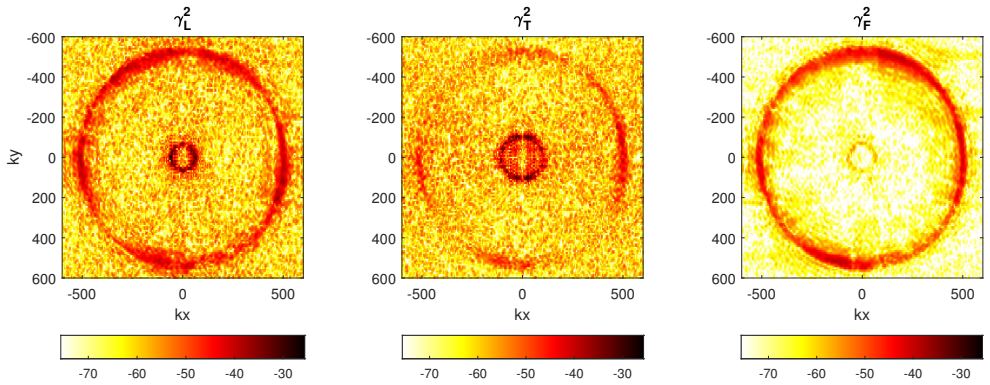

Figure 5: Wavenumber representation of γ_L^2, γ_T^2 and γ_F^2 at 49kHz.

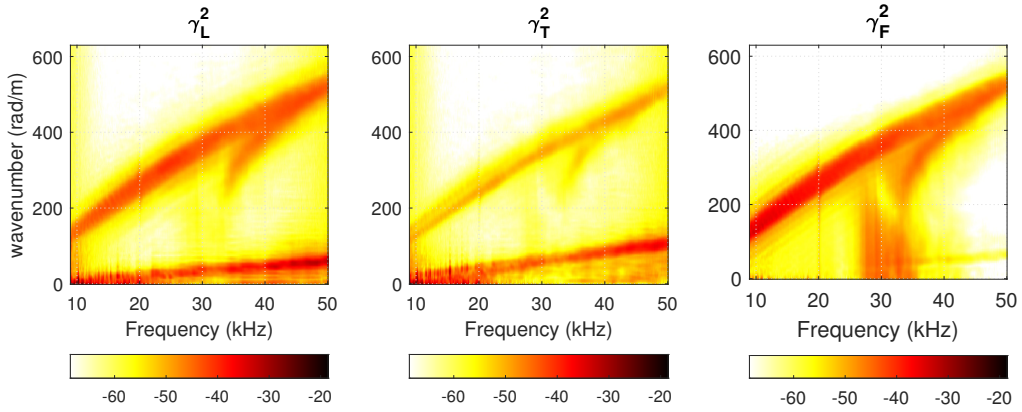

Figure 6: Frequency-Wavenumber map of γ_L^2, γ_T^2 and γ_F^2.

contribute to the transverse correlation ($\gamma_{FT}^2 = 0$ as seen in the theoretical section). Even if it still appears on these results, it is strongly attenuated as compared to U_x and U_y wavenumber maps. The transverse waves ridge, well seen on the $\gamma_T^2 = 0$ map, is completely absent on γ_L^2 and γ_F^2 maps.

2.4 Comparison with the Lamb model

The Lamb waves model describe the natural vibration mode of a plate structure. The model uses the Helmholtz decomposition to decouple the longitudinal and transverse components of the displacement field and solve their respective wave equations independently. The coupling between the longitudinal and transverse solutions is introduced by stress-free boundary conditions on both side of the plate. In case of a multilayer, additional stress and displacement couplings at the interfaces of the layers can be obtained. The dispersion curves of the structure are then identified by solving these coupled equations (see [3] for more details).

In the figure below, the dispersion curves estimated by the Lamb wave model are compared with the correlation coefficients in the frequency-wavenumber map. The flexural mode, which has the highest natural wavenumber over the whole frequency band, corresponds to the first antisymmetric mode of the Lamb wave model. The curve which has a cut-off frequency of approximately 33 kHz and reaches the flexural mode at higher frequency corresponds to the first symmetric mode (breathing mode). This mode is also visible on

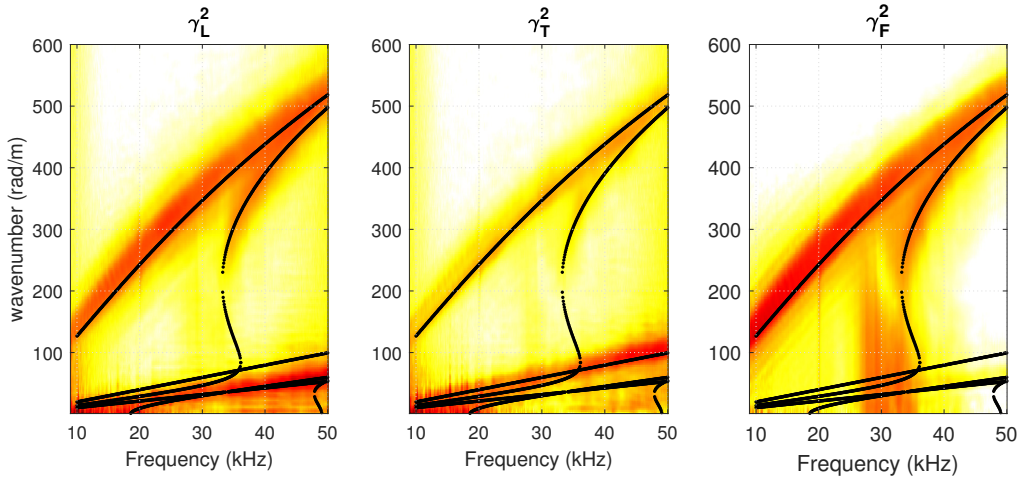

Figure 7: Comparison of the estimations of the Lamb waves model with the Frequency-Wavenumber map of γ_L^2, γ_T^2 and γ_F^2.

the correlation map. Finally, the dispersion curves of the longitudinal and transversal waves are also well identified by the Lamb wave model.

2.5 Experimental estimation of the coupling coefficient

It is clear, looking at the wavenumber content of the three components of the velocity field, that there exist a significant coupling effect between in-plane and out-of-plane vibrations, especially concerning the flexural waves that contributes quite strongly to in-plane vibration. At low frequency, for homogeneous thin plates without shearing, the coupling coefficient α correspond to half the plate thickness. For multi-layer structures, at mid and high frequencies, the coefficient can be significantly different because of in-plane shearing effects. The vectorial (3D) measurements allow the experimental estimation of α. For the wavenumber components corresponding to flexural waves (see Eq. (3), $\mathbf{F}$), one can write

$$U_x = -\alpha i k_x U_z \quad , \quad U_y = -\alpha i k_y U_z. \tag{6}$$

Writing as a system of equations these two equations for a subset of the wavenumber map corresponding to flexural waves, one can get a least square estimate of α

$$\alpha_{LS} = i \frac{\sum \left(k_x \overline{U_z} U_x + k_y \overline{U_z} U_y \right)}{\sum \left(k_x^2 |U_z|^2 + k_y^2 |U_z|^2 \right)} = i \frac{\sum \overline{U_z} \left(k_x U_x + k_y U_y \right)}{\sum |U_z|^2 k^2} \tag{7}$$

where $\overline{U}$ denotes the complex conjugate of U.

At each frequency, a subset of wavenumber components is selected based upon an energy criterion, and α_{LS} is calculated. The result is drawn in Fig. 8, separating the real and imaginary parts. The LS estimate is normalized with respect to the theoretical value for a homogeneous thin plate without shearing ($h/2$).

The first observation is that the LS estimation of α is relatively stable as a function of the frequency, and turns out to be a positive real coefficient, as expected. However, its value lies around 0.2 and 0.3, which is significantly lower than unity that would have been expected for a homogeneous thin plate (at low frequencies). This observation confirms the importance of the role of the shearing of the core in the dynamic of the sandwich structure on the whole studied frequency range. The comparison of this result with advanced models is left for future work.

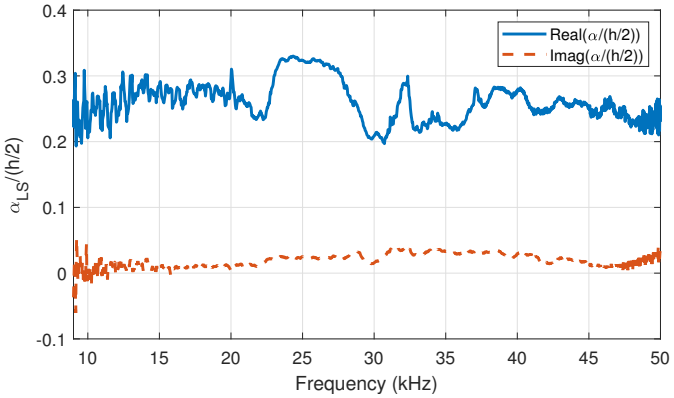

Figure 8: Least squares estimate of the α coefficient from vectorial (3D) velocity fields measurements, normalized by its value for a thin homogeneous plate without shearing (half plate thickness $h/2$).

3 Conclusion

This work proposes a wave correlation approach for vectorial velocity fields measurements. First results are presented, illustrating the ability of the method to properly separate longitudinal and transverse in-plane waves. The experimental estimation of the coupling coefficient is another interesting result. It can help understanding the dynamics of waves travelling into the structures and validating models.

References

[1] J. Berthaut, M. Ichchou, and L. Jezequel, "K-space identification of apparent structural behaviour," *Journal of Sound and Vibration*, vol. 280, no. 3, pp. 1125–1131, 2005. [Online]. Available: https://www.sciencedirect.com/science/article/pii/S0022460X04002925

[2] N. Roozen, Q. Leclère, K. Ege, and Y. Gerges, "Estimation of plate material properties by means of a complex wavenumber fit using hankel's functions and the image source method," *Journal of Sound and Vibration*, vol. 390, pp. 257–271, 2017. [Online]. Available: https://www.sciencedirect.com/science/article/pii/S0022460X16307118

[3] F. Marchetti, "Modélisation et caractérisation large bande de plaques multicouches anisotropes," Theses, Institut National des Sciences Appliquées de Lyon (INSA Lyon), Dec. 2019. [Online]. Available: https://tel.archives-ouvertes.fr/tel-02443702